International Journal of Inventive Engineering and Sciences (IJIES)
ISSN: 2319-9598 (Online), Volume-12 Issue-10, October 2025

Distinction Direction of Flux for PMs Used to Analyze Slotless Linear Motors with Buried PMs with Considering Finite Iron Core for HEVs Usages

Ehsan Shirzad

Abstract: ***The purpose of this paper is to present a mathematical model of the magnetic field distribution in planar linear buried permanent-magnet (PM) synchronous motors. The suggested strategy is based on 2D and can be utilized in any slotless linear buried PM machine that has any number of phases, remarkable advantage of buried PMs is high-speed capability due to planar force of zero at motion also, no need of epoxy resin glue to hold despite surface mounted linear PMSMs. The motor uses PDEs for seven regions to formulate its partial differential equations (PDEs): mover-side exterior, mover back iron, PMs, air-gap, winding, stator back-iron and stator-side exterior. Four different magnetization patterns, i.e. parallel, ideal Halbach, 2-segment Halbach and bar magnets in shifting directions magnetization patterns are considered to calculate the tangential and normal components of the open-circuit magnetic flux density, and armature response of the motor below the examination. The winding brings on voltage, flux linkage, self- and mutual inductances, and standard and tangential components of force are computed. The validity of the proposed method is shown by comparing the analytical results with those obtained from 2D finite-element analysis.***

Index Terms: ***2D Analytical Model, Buried PMs, Finite Element Method, Meshing, Vector Potential***

Nomenclature:
PMSMs: Permanent Magnet Synchronous Motors
HEVs: Hybrid Electric Vehicles
EVs: Electric Vehicles
PDEs: Partial Differential Equations

I. INTRODUCTION

Linear motors can produce direct thrust with no mechanical conversion from rotational to translational motion. In an electromagnetic device, the absence of mechanical conversion elements, such as gears, ball screws, and crankshafts, can significantly enhance overall machine performance by improving agility, reliability, maintenance, efficiency, and pressure density. Linear electric-powered machines are manufactured in both planar (flat) and tubular forms. almost any rotational electric powered machine (which includes DC, induction and synchronous machines) has its linear counterpart [1]. Furthermore, Permanent Magnet Synchronous Motors (PMSMs) have attracted significant attention in the field of Hybrid Electric Vehicles.

Manuscript received on 28 September 2025 | Revised Manuscript received on 04 October 2025 | Manuscript Accepted on 15 October 2025 | Manuscript published on 30 October 2025.
*Correspondence Author(s)
Ehsan Shirzad*, Department of Electrical Engineering, University of Bojnord, Bojnord, (North Khorasan), Iran. Email ID: Ehsan_shirzad_72@yahoo.com, ORCID ID: 0000-0003-3257-3754

© The Authors. Published by Blue Eyes Intelligence Engineering and Sciences Publication (BEIESP). This is an open-access article under the CC-BY-NC-ND license http://creativecommons.org/licenses/by-nc-nd/4.0/

(HEVs) and Electric Vehicles (EVs) because of their high torque-to-weight ratio, compact structure, and excellent controllability.

In HEVs, PMSMs are primarily used as traction motors and generators, converting electrical energy from the battery into mechanical motion and recovering energy during braking through regenerative operation. The high efficiency and precise torque control of PMSMs make them ideal for dynamic driving conditions that require frequent acceleration and deceleration.

In addition, the linear configuration of PMSMs has opened new possibilities for specific HEV subsystems such as active suspension systems, electromagnetic braking units, and linear actuators for steering or valve control. The absence of mechanical transmission elements in linear motors enables faster response times and lower maintenance, aligning with the automotive industry's goals of increasing reliability and reducing system complexity.

The analytical modelling of linear PMSMs, as presented in this paper, can therefore be extended to improve the design of HEV auxiliary systems where precise force generation and compact design are essential. Accurate estimation of magnetic flux distribution, force density, and induced-voltage characteristics helps engineers optimise energy efficiency and thermal management in hybrid powertrains. Recent studies have also demonstrated that buried or Halbach-type magnet arrangements in PMSMs enhance flux concentration and reduce cogging forces, both of which are critical for achieving quiet, smooth, and vibration-free operation in modern HEV systems.

Consequently, the continuous development of advanced analytical and finite-element models for PMSMs supports the automotive sector's transition toward sustainable, electrified transportation by enabling higher performance, lower energy losses, and more compact electromechanical designs.

Linear synchronous machines may be divided into electrically excited synchronous machines, permanent magnet synchronous machines (PMSMs), and synchronous reluctance machines, as shown in Fig. 1(a)-(c), respectively. Amongst the various excitation systems of synchronous machines, PMSMs, due to their significant benefits (high performance, compact structure, and positional accuracy), are widely used in speed- and position-controlled power systems, including in manufacturing automation systems and semiconductor manufacturing equipment [2][3][4]. The armature winding may be with or without armature slots. within the former, as proven in Fig. 1, the armature windings are inserted in the slots and in the latter, as demonstrated in Fig. 2, the armature windings are placed on the floor of the armature lower back-iron in buried PMs in mover,

© Copyright: All rights reserved.

between each PM and iron bridge with magnetic flux density of zero is considered to maximize magnetic flux density in airgap to enhance torque and minimize distortion. The slotted armature structure produces detent force, which is detrimental to device performance [5]. In linear PMSMs with a slotted armature, detent forces can be reduced by appropriately selecting the pole/slot combination or by skewing the armature slots or the PMs. The slotless armature structure is a strategy to eliminate detent force.

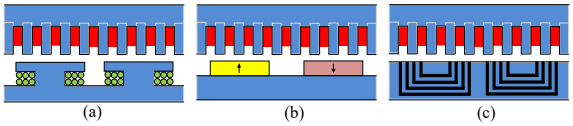

[Fig.1: (a) Electrically Excited Synchronous; (b) Permanent Magnet Synchronous; and (c) Synchronous Reluctance Machines]

An accurate electromagnetic model is vital to predict the overall performance of an electrical device [6-7]. The governing partial differential equations (PDEs) are derived using Maxwell's equations. The magnetic field of a linear electrical system can be determined both analytically and numerically [7-8]. An analytical version is notably faster because it has a lower computational burden than the numerical method. Design optimization of a linear permanent-magnet device considers both analytical and numerical processes in my view, or simultaneously [8-10]. but, analytical techniques, if possible, are desired, particularly when numerous hundreds of optimization iterations are necessary.

The analytical calculations of electromagnetic fields in linear electrical machines had been subjects of previously posted works [11][12][13][14] but, within the proposed techniques the finite permeability of the center materials has now not been considered and the effects are distinct to a specific magnetization pattern. The effects of armature reaction have not been considered, and the magnetic flux distribution is due solely to the PM. The analytical consequences in these works have been further confined to the calculation of overall performance quantities. Consequently, the results were limited to the calculation of both caused voltage, inductance or pressure [17-18]. As such, these days, in [15], the authors have presented a 2d analytical version for slotted planar permanent-magnet linear synchronous machines and only armature reaction flux distribution turned into investigated. In [16]. recently the authors have proposed an analytical version for slotted and slotless linear machines. Still, the permeability of the stator and mover lower back irons was assumed to be infinite, and the simplest parallel magnetisation model was adopted.

In this paper, an accurate two-dimensional (2D) analytical approach for calculating the electromagnetic area of linear planar slotless PMSMs is proposed. The key modification from previous works is the inclusion of finite core permeability. Secondly, this examines 4 unique magnetisation styles — i.e., parallel, perfect Halbach, 2-phase Halbach, and bar magnets — in transfer instructions. Eventually, this look includes calculations of dynamic performance parameters, such as forces, flux linkage, back emf, and inductances. It also calculates the open-circuit and armature-reaction magnetic subject distributions.

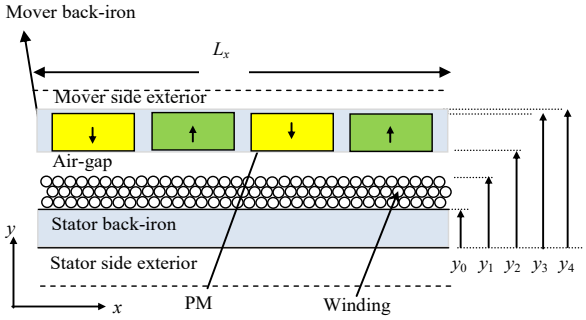

[Fig.2: Geometry and Regions of the Buried Linear PMSM]

II. METHODOLOGY

An electromagnetic problem is initiated by invoking a set of assumptions to allow the analytical solution of the governing partial differential equations (PDEs) derived from Maxwell's equations. Magnetization patterns and distribution of the armature current density are expressed in terms in their Fourier series expansions. In this paper, the components are based entirely on the magnetic vector potential, yielding a fixed set of Laplace and Poisson equations. Based on the governing equations and a set of boundary conditions, a general solution is assigned to each sub-place. Fig. 2 shows the geometry of the linear PM synchronous machine, which includes seven sub-areas: mover-facet exterior, mover lower back iron, PMs, airgap, winding, stator back-iron, and stator-aspect exterior. Assumption for solving is as follows:

$$\boldsymbol{A} = [0, 0, A_z(x,y)]$$
$$\boldsymbol{M} = [M_x(x), M_y(x), 0]$$
$$\boldsymbol{B} = [B_x(x,y), B_y(x,y), 0]$$

- all substances are isotropic;
- the media have finite permeability;
- the saturation outcomes are overlooked;
- the motor has a slotless stator structure;
- Eddy contemporary reaction field is neglected.

A. Governing PDEs

The simple equations, which describe the quasi-static electromagnetic issues, are primarily based on Maxwell's equations:

$$\nabla \times \boldsymbol{H} = \boldsymbol{J} \quad (1)$$
$$\nabla \cdot \boldsymbol{B} = 0 \quad (2)$$

where $\boldsymbol{H}$ is the magnetic field intensity vector, $\boldsymbol{J}$ is the armature current density vector, which is zero in open-circuit field calculations, and B is the magnetic flux density vector. Simplifying the Maxwell equations results in the following equation:

$$-\nabla^2 \boldsymbol{A} = \mu_0 \mu_r \boldsymbol{J} + \mu_0 \nabla \times \boldsymbol{M} \quad (3)$$

The magnetic flux density is obtained by taking the curl of the magnetic vector potential. Assuming 2D analysis in Cartesian coordinates, the above expression can be rewritten in the following expansion form for region:

© Copyright: All rights reserved.

$$-\frac{\partial^2 A_z^i}{\partial x^2}-\frac{\partial^2 A_z^i}{\partial y^2}=\mu_0\mu_r J_z^i + \mu_0\left(\frac{\partial M_y^i}{\partial x}-\frac{\partial M_x^i}{\partial y}\right) \quad (4)$$

where$i=\{em, m, pm, a, w, s, es\}$ indicates the mover side exterior, mover, magnet, air-gap, winding, stator back-iron and stator side exterior sub-regions, respectively. Therefore, the above expression for the exterior, mover, airspace and stator back-iron sub-regions can be rewritten as:

$$-\frac{\partial^2 A_z^i}{\partial x^2}-\frac{\partial^2 A_z^i}{\partial y^2}=0 \qquad i=\{em,m,a,s,es\} \quad (5)$$

for the winding sub-region, equation (4) is expressed as:

$$-\frac{\partial^2 A_z^w}{\partial x^2}-\frac{\partial^2 A_z^w}{\partial y^2}=\mu_0 J_z \quad (6)$$

and for the PMs sub-region, equation (4) is expressed as:

$$-\frac{\partial^2 A_z^{pm}}{\partial x^2}-\frac{\partial^2 A_z^{pm}}{\partial y^2}=\mu_0\left(\frac{\partial M_y}{\partial x}-\frac{\partial M_x}{\partial y}\right) \quad (7)$$

In this paper, solutions to both the open-circuit magnetic field problem and the armature reaction field problem are presented.

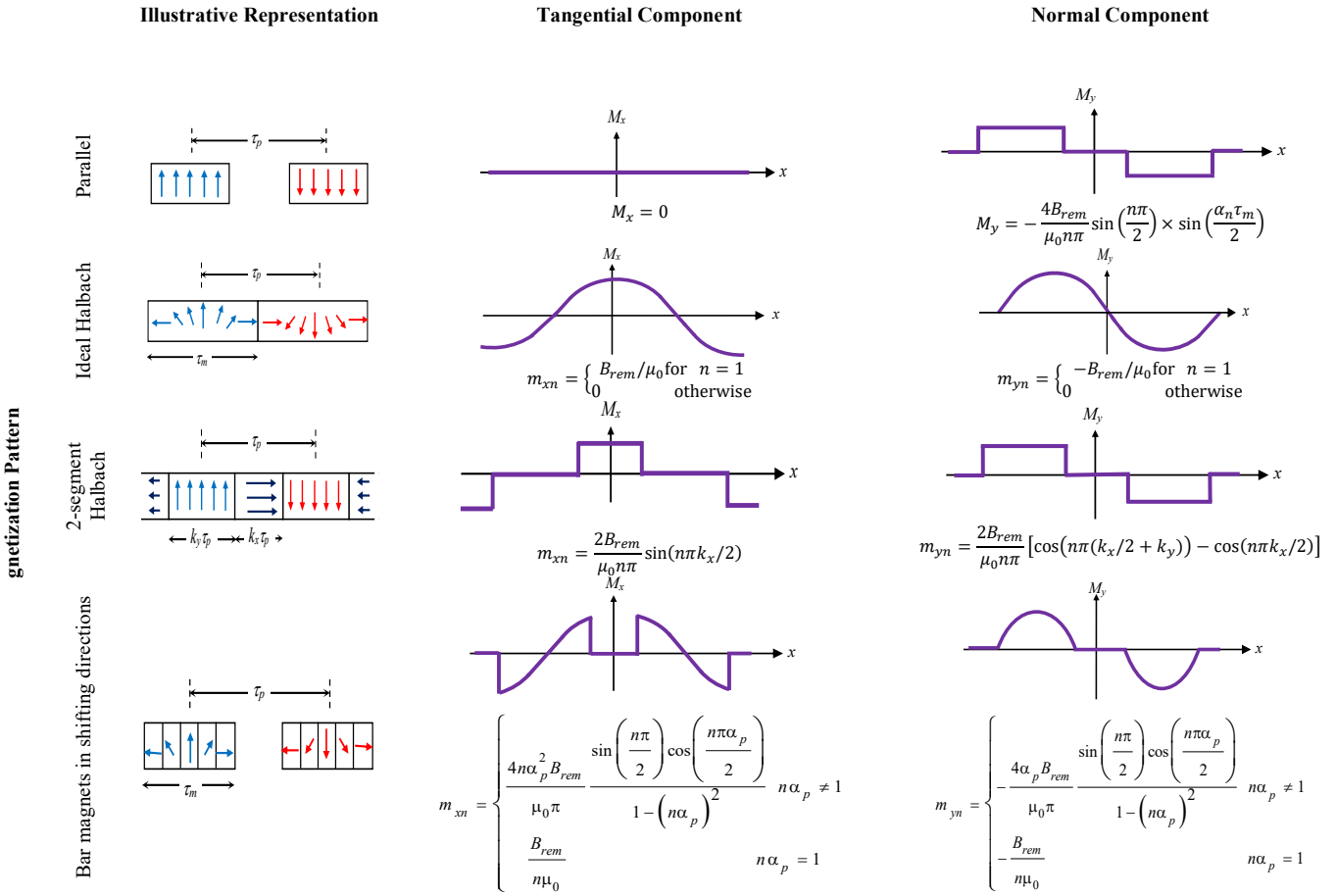

k_x and k_y are the x-direction magnetized PM width to the pole pitch ratio and the y-direction magnetized PM width to the pole pitch ratio, respectively
B_{rem} is the permanent magnet remanence flux density
τ_m is the magnet width
$\alpha_p = \tau_m/\tau_p$

[Fig.3: Illustrative Illustration of the PM Magnetizations with Their Tangential and Normal Additives [26-27]]

B. General Formulation and Solution

In this take a look at, the use of the method of Separation of Variables yields a widespread solution for the Laplace/Poisson equation in every sub-region. consistent with (5), the general solution for em, m, a, s, es sub-regions is as follows:

$$A_z^i(x,y)=\sum_{n=1}^{\infty}(a_n^i e^{\alpha_n y}+b_n^i e^{-\alpha_n y})\cos(\alpha_n x) + (c_n^i e^{\alpha_n y} + d_n^i e^{-\alpha_n y})\sin(\alpha_n x) \quad (8)$$

where$\alpha_n = n\pi/\tau_p$ and τ_p is the pole pitch. The flux density vector in all the sub-regions is then obtained by curling the magnetic vector potential.

$$\mathbf{B} = \nabla \times \boldsymbol{A} \quad (9)$$

Before expressing the general solution to the Poisson equation in the PM sub-area, the magnetisation distribution of the magnets must be provided. In Cartesian coordinates, the magnetization vector of a PM is expressed with the aid of its normal and tangential additives. Representing the normal and tangential components of the

© Copyright: All rights reserved.

magnetisation patterns in terms of their Fourier coefficients enables the analytical solution of the PDEs. The provided analytical model is based solely on the magnetisation styles in Fig. 3; however, the proposed approach applies to any voluntary magnetisation styles. Fig. 3 indicates the illustrative representation and the harmonic amplitudes of the tangential and regular additives for the parallel, perfect Halbach, 2-phase Halbach and bar magnets in shifting course magnetization styles, respectively. Assume the origin of x-axis is aligned with the PM neutral axis, the Fourier series expansions of the tangential and normal components of any magnetization pattern are expressed as:

$$M_x(x) = \sum_{n=1}^{\infty} m_{xn} \cos(\alpha_n x) \tag{10}$$

$$M_y(x) = \sum_{n=1}^{\infty} m_{yn} \sin(\alpha_n x) \tag{11}$$

Based on equation (7) and the Fourier series expansion of the magnetization pattern, the combined general and particular solution for the PM elementsub-region is expressed as:

$$A_z^{pm}(x,y) = \sum_{n=1}^{\infty} (a_n^{pm} e^{\alpha_n y} + b_n^{pm} e^{-\alpha_n y} + \frac{\mu_0}{\alpha_n} m_{yn}) \times \cos(\alpha_n x) + (c_n^{pm} e^{\alpha_n y} + d_n^{pm} e^{-\alpha_n y}) \times \sin(\alpha_n x) \tag{12}$$

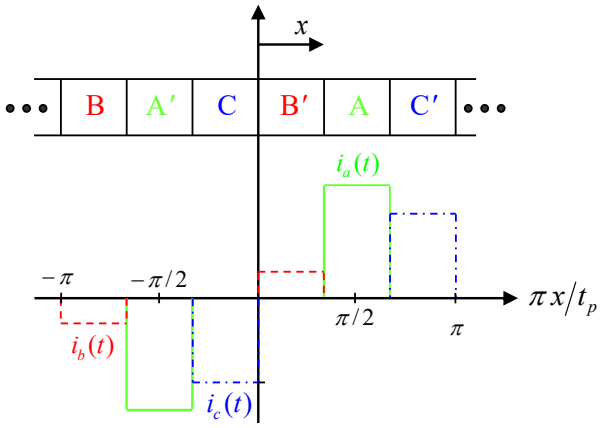

Fig.4: Spatial Current Distribution of a Three-Phase Full-Pitch Winding]

In an effort to comprise the movement of the mover, the displacement of the mover is expressed as follows:

$$\delta = vt + \delta_0 \tag{13}$$

where$v$ is the velocity of the mover assumed to be constant, t is the time, $\delta_0$is the initial position of the mover with respect to the armature. Therefore, in all the expressions of the mover and PM sub-regions, i.e. (8)-(12), x is replaced by $x - \delta$.

To locate the overall and specific answers within the winding sub-vicinity, a 3-phase armature contemporary density distribution, as proven in Fig. four, is presented via the following Fourier series expansion:

$$J_z(x,t) = \sum_{n=1}^{\infty} J_{1n} \sin(\alpha_n x) + J_{2n} \cos(\alpha_n x) \tag{14}$$

were

$$J_{1n} = -\frac{2 N_t \tau_p}{3(y_1 - y_0)} \frac{\cos(\frac{2n\pi}{3}) - \cos(\frac{n\pi}{3})}{n\pi} \times (i_a(t) + i_b(t)\cos(\frac{2n\pi}{3}) + i_c(t)\cos(\frac{2n\pi}{3})) \tag{15}$$

$$J_{2n} = -\frac{2 N_t \tau_p}{3(y_1 - y_0)} \frac{\cos(\frac{2n\pi}{3}) - \cos(\frac{n\pi}{3})}{n\pi} \times (-i_b(t)\sin(\frac{2n\pi}{3}) + i_c(t)\sin(\frac{2n\pi}{3})) \tag{16}$$

where N_t is the number of turns for each coil calculated as:

$$N_t = \frac{k_f (y_1 - y_0)\tau_p}{3A_c} \tag{17}$$

$k_f$is the filling factor and A_c is the cross-sectional area of the wire and y_0 is the interface between the stator and winding sub-regions and $y_1$is the interface between the winding and air-gap sub-regions. The currents of the three-phase windings are assumed as follows:

$$i_a(t) = I_m \sin\left(\frac{v}{\tau_p}\pi t\right) \tag{18}$$

$$i_b(t) = I_m \sin\left(\frac{v}{\tau_p}\pi t - \frac{2\pi}{3}\right) \tag{19}$$

$$i_c(t) = I_m \sin\left(\frac{v}{\tau_p}\pi t + \frac{2\pi}{3}\right) \tag{20}$$

whereI_m is the peak of the armature current. Therefore, in the winding sub-region, the solution is obtained as:

$$A_z^w(x,y) = \sum_{n=1}^{\infty} (a_n^w e^{\alpha_n y} + b_n^w e^{-\alpha_n y} + \frac{\mu_0}{\alpha_n^2} J_{2n}) \times \cos(\alpha_n x) + (c_n^w e^{\alpha_n y} + d_n^w e^{-\alpha_n y} + \frac{\mu_0}{\alpha_n^2} J_{1n}) \times \sin(\alpha_n x) \tag{21}$$

It is to be noted that the magnetic vector potential is calculated in various sub-regions. Therefore, the components of the magnetic flux density vector can be achieved by equation (9).

C. Boundary Conditions

The regular issue of the magnetic flux density vector is continuous across the interface between two adjacent media. In the case of a supply-free interface, the parallel component of the magnetic field intensity vector is continuous across that interface. Therefore, the boundary/interface situations for the slotless planar linear PM synchronous motors are:

$$H_x^i(x,y)\big|_y = H_x^{i+}(x,y)\big|_y \tag{22}$$

$$B_y^i(x,y)\big|_y = B_y^{i+}(x,y)\big|_y \tag{23}$$

According to the geometry considerations and the defined coordinate system, some of the integral constants must be zero (i.e., a i.e.$a_n^{em} = c_n^{em} = b_n^{es} = d_n^{es} = 0$). After

Published By:
Blue Eyes Intelligence Engineering and Sciences Publication (BEIESP)
© Copyright: All rights reserved.

implementing the boundary conditions, a set of 24 simultaneous algebraic equations is formed. The unknown variables

are: $b_n^{em},\ d_n^{em},\ a_n^m, b_n^m, c_n^m, d_n^m, a_n^{pm},\ b_n^{pm}, c_n^{pm}$
$d_n^{pm},\ a_n^a,\ b_n^a, c_n^a, d_n^a,\ a_n^w,\ b_n^w, c_n^w, d_n^w, a_n^s,\ b_n^s, c_n^s,\ d_n^s, a_n^{es},$
c_n^{es}. The simultaneous algebraic equations are given in Appendix 1.

III. CASE STUDY

To validate the derived expressions, the magnetic field distribution in diverse sub-regions of a linear buried PM synchronous motor is calculated and compared with that obtained from finite-element analysis. Desk II in Appendix 2 lists the specs of the linear motor under the test. The magnetic flux density vector includes components, tangential path denoted by way of subscript "x" and ordinary path denoted by way of subscript "y". These two components are computed for all sub-regions using both analytical and finite-element methods.

A. Magnetic Flux Density Distribution

Fig. 5 shows the analytical open-circuit magnetic flux density distribution of the motor under observation for various magnetisation patterns. As such, the tangential and ordinary components of the magnetic flux density, obtained analytically in distinct sub-regions, are compared with the numerically calculated values.

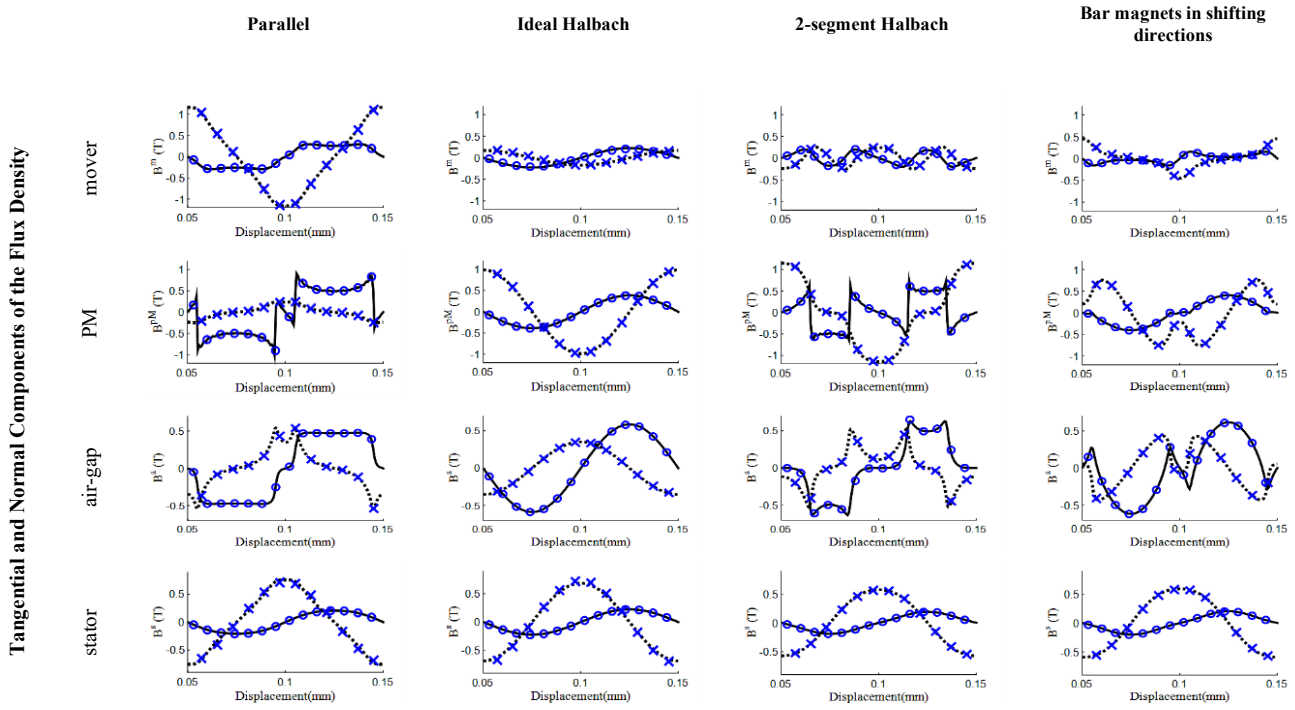

Numerical results of the standard component of flux density
times Numerical results of the tangential component of flux density
...Analytical results of the tangential component of flux density
minus Analytical results of the standard component of flux density

[Fig.5: Analytical and Numerical Open-Circuit Magnetic Flux Density Distribution of the Motor Under the Take a Look at with Distinct Magnetization Patterns]

The magnetic flux density within the mover back iron of the motor with parallel magnetisation is higher than that of machines with different Halbach magnetisation patterns. It's mainly due to the tendency of the flux lines to skip through the PM sub-vicinity for the vehicles with ideal Halbach, 2-segment Halbach, and bar magnet in the moving path styles. The tendency of the magnetisation closer to the proper Halbach sample results in a greater sinusoidal airgap flux density.

Fig. 6 indicates the analytical and numerical results of the flux density distribution originated from the armature response, Flux Linkage and induced Voltage

The flux linkage is calculated from the flux density inside the winding sub-region due to the existence of PMs as follows:

$$\lambda_a = N_t N_c \int \boldsymbol{B} \cdot d\boldsymbol{s} = N_t N_c L_z \int_{x_2}^{x_1} B_y \, dx \qquad (23)$$

where λ_a is the flux linked with phase "a" and B_y is the standard component of the winding flux density, x_2 and x_1 are the middle position of the coil-sides of the first coil. N_c is the number of coils in each phase and L_z is the machine depth.

By using Faraday's law, the induced voltage in phase "a" is obtained as follows:

$$e_a = \frac{d\lambda_a}{dt} \qquad (24)$$

Published By:
Blue Eyes Intelligence Engineering
and Sciences Publication (BEIESP)
© Copyright: All rights reserved.

...Analytical results of the tangential component of flux density

—Analytical results of the standard component of flux density

Numerical results of the standard component of flux density

times Numerical results of the tangential component of flux density

[Fig.6: Analytical and Numerical Magnetic Flux Density Distribution Originated from Armature Reaction of the Motor Under the Study]

B. Magnetic Force Calculations

To calculate the tangential and normal components of the magnetic forces, Maxwell's stress tensor method is utilized as follows:

$$F_x = \frac{L_z}{\mu_0}\int_{-\frac{L_x}{2}}^{\frac{L_x}{2}} B_x B_y dx \qquad (25)$$

$$F_y = \frac{L_z}{2\mu_0}\int_{-\frac{L_x}{2}}^{\frac{L_x}{2}} (B_x^2 - B_y^2) dx \qquad (26)$$

whereB_x and B_y are the tangential and normal components of the flux density in the air-gap sub-region, respectively.

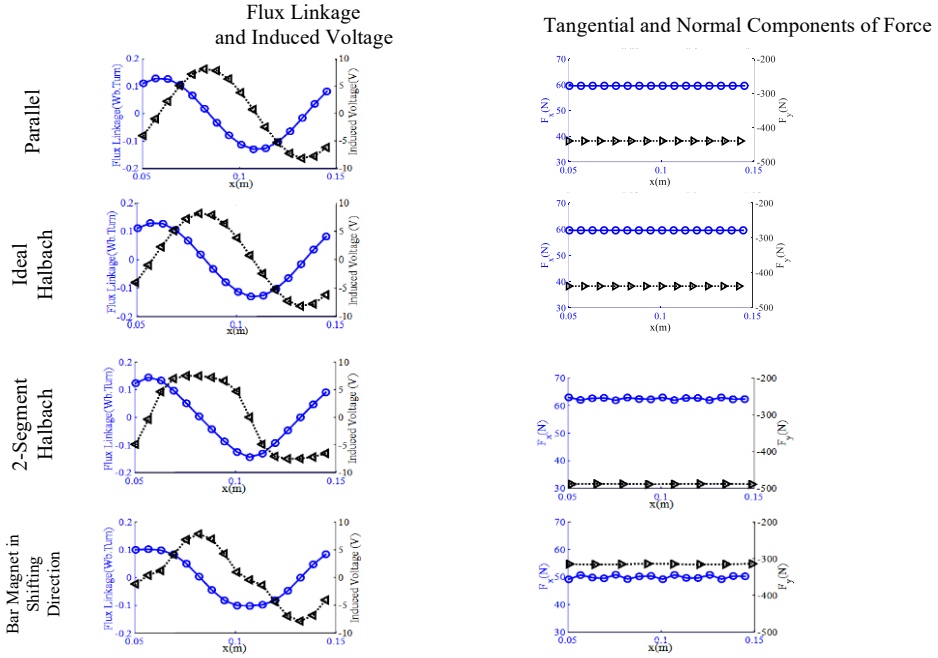

O λ_a Numeric Δ e_a Numeric O F_x Numeric Δ F_y Numeric

$-\lambda_a$ Analytic ..e_a Analytic$-F_x$ Analytic..F_y Analytic

[Fig.7: Analytical and Numerical Calculation of the Flux Linkage, Induced Voltage, Tangential and Normal Components of Magnetic Force]

Fig. 7 compares the analytically and numerically calculated flux linkages, induced voltages, and the tangential and normal components of the electromagnetic forces of the linear motor under consideration for specific PM magnetisations. The applied force (Fx) on the windings is consistent due to the test machine's slotless structure and sinusoidal armature current. The troops (Fy) in your course are poor because the result of PMs attracting the stator back iron violates the third Newton law.

C. Inductances

Neglecting saturation effects, the inductances are independent of the armature current. Also, because of the steady magnetic air-gap length in an established shape, the inductances are independent of the mover position. Therefore, the self-inductance is calculated at a single mover role using the subsequent expression:

© Copyright: All rights reserved.

$$L_{aa} = \frac{\lambda_{aa}}{i_a} \tag{27}$$

whereL_{aa} is the self-inductance of the first phase and i_a is the applied armature current in the first phase and λ_{aa} is the flux linked with the winding of the first phase due only to the first-phase armature current?

IV. CONCLUSION

An accurate analytical calculation of the magnetic field for a slotless linear PM synchronous motor has been provided. the answer was based on the utilisation of 2D magnetic field analysis, which considered four distinct magnetisation patterns: parallel, perfect Halbach, 2-segment Halbach, and bar magnets in transfer directions. The analytical expressions for the magnetic flux density (due to PM and armature reaction), flux linkage, self- and mutual inductances, back-emf, and force were derived. The agreement between the finite element results and the analytical solutions fully validates the proposed analytical method. The proposed technique is well-known and applicable to a voluntary slotless linear PM motor with arbitrary permanent magnet and winding configurations.

Each analytical and finite element effects display that the mover lower back-iron does no longer play a element within the flux path of the perfect Halbach magnetization sample in the slotless form of the linear PM synchronous motor. it is therefore possible to analyse the elimination of the mover back-iron or its replacement with a different material that's lighter or has a higher heat-dissipation ability than iron. Minimum harmonics in the flux density and flux linkage, and, as a result, lower back-emf, were observed for the motor with an ideal Halbach magnetisation sample compared to alternative magnetisation styles. It was also discovered that the armature reaction has a negligible effect on the everyday stress in a slotless motor.

V. APPENDIX

Appendix1

Implementing the boundary situations related to the tangential problem of the magnetic region depth and ordinary problem of flux density at the interface between each sub-region yields the following equations:

A. Interface Between the Mover-Side Exterior and Mover Regions

$$-\mu_r^m b_n^{em} e^{-\alpha_n y_4} - a_n^m e^{\alpha_n y_4} + b_n^m e^{-\alpha_n y_4} = 0 \tag{28}$$

$$-\mu_r^m d_n^{em} e^{-\alpha_n y_4} - c_n^m e^{\alpha_n y_4} + d_n^m e^{-\alpha_n y_4} = 0 \tag{29}$$

$$-b_n^{em} e^{-\alpha_n y_4} + a_n^m e^{\alpha_n y_4} + b_n^m e^{-\alpha_n y_4} = 0 \tag{30}$$

$$d_n^{em} e^{-\alpha_n y_4} - c_n^m e^{\alpha_n y_4} - d_n^m e^{-\alpha_n y_4} = 0 \tag{31}$$

B. Interface Between the Mover and Magnet Sub-Regions

$$\begin{aligned} &\mu_r^{pm} a_n^m e^{\alpha_n y_3} - \mu_r^{pm} b_n^m e^{-\alpha_n y_3} \\ &\quad - \mu_r^m a_n^{pm} e^{\alpha_n y_3} + \mu_r^m b_n^{pm} e^{-\alpha_n y_3} = \\ &\quad \frac{-\mu_r^m \mu_0 m_{xn}}{\alpha_n} \cos(\alpha_n \delta) \end{aligned} \tag{32}$$

$$\begin{aligned} &\mu_r^{pm} c_n^m e^{\alpha_n y_3} - \mu_r^{pm} d_n^m e^{-\alpha_n y_3} \\ &\quad - \mu_r^m c_n^{pm} e^{\alpha_n y_3} + \mu_r^m d_n^{pm} e^{-\alpha_n y_3} = \\ &\quad - \frac{\mu_r^m \mu_0 m_{xn}}{\alpha_n} \sin(\alpha_n \delta) \end{aligned} \tag{33}$$

$$\begin{aligned} &-a_n^m e^{\alpha_n y_3} - b_n^m e^{-\alpha_n y_3} \\ &\quad + a_n^{pm} e^{\alpha_n y_3} + b_n^{pm} e^{-\alpha_n y_3} = \\ &\quad - \frac{\mu_0 m_{yn}}{\alpha_n} \cos(\alpha_n \delta) \end{aligned} \tag{34}$$

$$\begin{aligned} &c_n^m e^{\alpha_n y_3} + d_n^m e^{-\alpha_n y_3} \\ &\quad - c_n^{pm} e^{\alpha_n y_3} - d_n^{pm} e^{-\alpha_n y_3} = \\ &\quad \frac{\mu_0 m_{yn}}{\alpha_n} \sin(\alpha_n \delta) \end{aligned} \tag{35}$$

C. Interface Between the Magnet and Air-Gap Sub-Regions

$$\begin{aligned} &a_n^{pm} e^{\alpha_n y_2} - b_n^{pm} e^{-\alpha_n y_2} \\ &\quad - \mu_r^{pm} a_n^a e^{\alpha_n y_2} + \mu_r^{pm} b_n^a e^{-\alpha_n y_2} = \\ &\quad \frac{\mu_0 m_{xn}}{\alpha_n} \cos(\alpha_n \delta) \end{aligned} \tag{36}$$

$$\begin{aligned} &c_n^{pm} e^{\alpha_n y_2} - d_n^{pm} e^{-\alpha_n y_2} \\ &\quad - \mu_r^{pm} c_n^a e^{\alpha_n y_2} + \mu_r^{pm} d_n^a e^{-\alpha_n y_2} = \\ &\quad - \frac{\mu_0 m_{xn}}{\alpha_n} \sin(\alpha_n \delta) \end{aligned} \tag{37}$$

$$\begin{aligned} &-a_n^{pm} e^{\alpha_n y_2} - b_n^{pm} e^{-\alpha_n y_2} \\ &\quad + a_n^a e^{\alpha_n y_2} + b_n^a e^{-\alpha_n y_2} = \\ &\quad \frac{\mu_0 m_{yn}}{\alpha_n} \cos(\alpha_n \delta) \end{aligned} \tag{38}$$

$$\begin{aligned} &c_n^{pm} e^{\alpha_n y_3} + d_n^{pm} e^{-\alpha_n y_3} \\ &\quad - c_n^a e^{\alpha_n y_3} - d_n^a e^{-\alpha_n y_3} = \\ &\quad - \frac{\mu_0 m_{yn}}{\alpha_n} \sin(\alpha_n \delta) \end{aligned} \tag{39}$$

D. Interface Between the Air-Gap and Winding Sub-Regions

© Copyright: All rights reserved.

$$a_n^a e^{\alpha_n y_1} - b_n^a e^{-\alpha_n y_1} - a_n^w e^{\alpha_n y_1} + b_n^w e^{-\alpha_n y_1} = 0 \quad (40)$$

$$c_n^a e^{\alpha_n y_1} - d_n^a e^{-\alpha_n y_1} - c_n^w e^{\alpha_n y_1} + d_n^w e^{-\alpha_n y_1} = 0 \quad (41)$$

$$-a_n^a e^{\alpha_n y_1} - b_n^a e^{-\alpha_n y_1} + a_n^w e^{\alpha_n y_1} + b_n^w e^{-\alpha_n y_1} = \frac{-\mu_0 J_{2n}}{\alpha_n^2} \quad (42)$$

$$c_n^a e^{\alpha_n y_1} + d_n^a e^{-\alpha_n y_1} - c_n^w e^{\alpha_n y_1} - d_n^w e^{-\alpha_n y_1} = \frac{\mu_0 J_{1n}}{\alpha_n^2} \quad (43)$$

E. Interface Between the Winding and Stator Sub-Regions

$$\mu_r^s a_n^w e^{\alpha_n y_0} - \mu_r^s b_n^w e^{-\alpha_n y_0} - a_n^s e^{\alpha_n y_0} + b_n^s e^{-\alpha_n y_0} = 0 \quad (44)$$

$$\mu_r^s c_n^w e^{\alpha_n y_0} - \mu_r^s d_n^w e^{-\alpha_n y_0} - c_n^s e^{\alpha_n y_0} + d_n^s e^{-\alpha_n y_0} = 0 \quad (45)$$

$$a_n^w e^{\alpha_n y_0} + b_n^w e^{-\alpha_n y_0} - a_n^s e^{\alpha_n y_0} - b_n^s e^{-\alpha_n y_0} = \frac{-\mu_0 J_{2n}}{a_n^2} \quad (46)$$

$$c_n^w e^{\alpha_n y_0} + d_n^w e^{-\alpha_n y_0} - c_n^s e^{\alpha_n y_0} - d_n^s e^{-\alpha_n y_0} = \frac{-\mu_0 J_{1n}}{a_n^2} \quad (47)$$

F. Interface Between the Stator and Stator-Side Exterior Sub-Regions

$$a_n^s - b_n^s + \mu_r^s b_n^{es} = 0 \quad (48)$$

$$c_n^s - d_n^s + \mu_r^s d_n^{es} = 0 \quad (49)$$

$$a_n^s + b_n^s - b_n^{es} = 0 \quad (50)$$

$$c_n^s + d_n^s - d_n^{es} = 0 \quad (51)$$

Note that to investigate the magnetic flux density originated from the PMs only, it is required to set the current density components to zero (i.e. $J_{1n} = J_{2n} = 0$). To investigate the armature reaction magnetic flux density, the magnetization components should be nullified (i.e. $M_{xn} = M_{yn} = 0$).

APPENDIX 2

The specifications of the linear PM synchronous motor as the case study are listed in Table I.

Table I: Specifications of the Single-Sided Linear PM Synchronous Motor

Parameters	Symbols	Values
Stator length	L_x	200 mm
Stator back iron height	y_0	10 mm
Winding height	$y_1 - y_0$	10 mm
Air-gap height	$y_2 - y_1$	2 mm
PM height	$y_3 - y_2$	8 mm
Mover back iron height	$y_4 - y_3$	10 mm
Stator relative permeability	μ_r^s	1000
Mover relative permeability	μ_r^m	1000
PM relative permeability	μ_r^{pm}	1.1
PM width for parallel pattern	τ_m	40 mm
Pole pitch	τ_p	50 mm
Number of poles	p	4
Motor depth	L_z	5 mm
x-direction magnetized PM width to the pole pitch ratio for 2-segment Halbach	k_x	0.4
y-direction magnetized PM width to the pole pitch ratio for 2-segment Halbach	k_y	0.6
PM Remanence flux density	B_{rem}	1.23 T
Peak armature current	I_m	5A
Number of turns per coil	N_t	83
Number of coils per phase	N_c	2
Cross-sectional area of wire	A_c	1mm^2
Filling factor	K_f	0.6
Velocity of the mover	v	1 m/s

DECLARATION STATEMENT

After aggregating input from all authors, I must verify the accuracy of the following information as the article's author.

- **Conflicts of Interest/ Competing Interests:** Based on my understanding, this article has no conflicts of interest.
- **Funding Support:** This article has not been funded by any organizations or agencies. This independence ensures that the research is conducted with objectivity and without any external influence.
- **Ethical Approval and Consent to Participate:** The content of this article does not necessitate ethical approval or consent to participate with supporting documentation.
- **Data Access Statement and Material Availability:** The adequate resources of this article are publicly accessible.
- **Author's Contributions:** The authorship of this article is contributed equally to all participating individuals.

REFERENCES

1. C. H. Ho and J.-C. Hwang, "Design of small permanent-magnet linear motors and drivers with integrated sensing," *Energies*, vol. 17, no. 22, 2024. [Online]. Available: (https://www.mdpi.com/1996-1073/17/22/5719)
2. Z. Li, L. Wu, X. Huang, and L. Peretti, "Hybrid analytical model of permanent magnet linear motor considering iron saturation and end effect," *IEEE Trans. Ind. Electron.*, 2023. [Online]. Available: (https://ieeexplore.ieee.org/document/10000000)
3. A. Bouzidi et al., "A review on analytical models of brushless permanent magnet machines," *ResearchGate*, 2023. [Online]. Available: (https://www.researchgate.net/publication/10000000)
4. J. Zhang, Z. Yang, M. Yu, and Y. Ye, "Analytical model for double-sided linear permanent magnet inner armature synchronous motors," *Arch. Electr. Eng.*, vol. 72, no. 3, 2023. [Online].

Published By:
Blue Eyes Intelligence Engineering and Sciences Publication (BEIESP)
© Copyright: All rights reserved.

Available: (https://www.researchgate.net/publication/372530317)
5. A. Dabiri, Y. Miloud, and M. Jallouli, "Optimal force control of a permanent magnet linear synchronous motor," *Mechatronics*, vol. 80, 2022. [Online]. Available: (https://www.sciencedirect.com/science/article/pii/S0957415822012345)
6. M. Vaezi, A. Hassani, and M. Tavakkoli, "A comprehensive review on the end effects of linear permanent magnet machines," *ResearchGate*, 2025. [Online]. Available: (https://www.researchgate.net/publication/10000000)
7. X. Li, D. Fang, and Q. Zhao, "A review on disturbance analysis and suppression for permanent magnet linear motors," *Machines*, vol. 10, no. 4, 2022. [Online]. Available: (https://www.mdpi.com/2075-1702/10/4/84)
8. Y. Zhang, X. Lu, and M. Huang, "Electromagnetic design and analysis of permanent magnet linear synchronous motor," *Energies*, vol. 15, no. 15, 2023. [Online]. Available: (https://www.mdpi.com/1996-1073/15/15/5441)
9. T. Lin, Y. Zhao, and K. Chen, "Linear tubular permanent magnet motor for an electromagnetic suspension system," *IET Electr. Power Appl.*, vol. 15, no. 3, 2021. [Online]. Available: (https://digital-library.theiet.org/content/journals/10.1049/elp2.12191)
10. A. Miller, "Manufacturing and testing the permanent magnet linear motor," *Linfield College Physics Senior Theses*, 2018. [Online]. Available: (https://digitalcommons.linfield.edu/physstud_theses/1)
11. F. Wang, Z. Yu, and R. Sun, "Analytical modeling and analysis of permanent magnet motor with demagnetization faults," *Sensors*, vol. 22, no. 23, 2022. [Online]. Available: (https://www.mdpi.com/1424-8220/22/23/9237)
12. F. Cui, Z. Sun, and K. Liu, "Comparative analysis of bilateral PMLSM structures with improved thrust density," *CES Trans. Electr. Mach. Syst.*, vol. 4, no. 3, 2020. [Online]. Available: (https://www.ces-transactions.com/)
13. H. Hu, X. Liu, J. Zhao, and Y. Guo, "Analysis and minimization of detent end force in permanent magnet linear motors," *IEEE Trans. Ind. Electron. *, vol. 65, no. 3, 2018. [Online]. Available: (https://ieeexplore.ieee.org/document/8048475)
14. S.-A. Kim, Y.-W. Zhu, and J.-K. Lee, "Electromagnetic normal force characteristics of linear machines with double primary side," *IEEE Trans. Magn. *, vol. 50, no. 5, 2014. [Online]. Available: (https://ieeexplore.ieee.org/document/6776500)
15. S.-G. Lee, S.-A. Kim, and D.-H. Park, "Optimal structure design for minimizing detent force of PMLSM," *IEEE Trans. Magn. *, vol. 50, no. 11, 2014. [Online]. Available: (https://ieeexplore.ieee.org/document/6974600)
16. Z. Chen, W. B. Kong, and Q. Wang, "Thrust force ripple reduction in PMLSM using dynamic harmonic current compensation," *IET Electr. Power Appl.*, vol. 14, no. 7, 2020. [Online]. Available: (https://digital-library.theiet.org/content/journals/10.1049/iet-epa.2019.0875)
17. E. Shirzad, H. Pirouz, and M. T. Shirzad, "Subdomain method for brushless double-rotor flux-switching permanent magnet machines with yokeless stator," *Electrical Engineering*, vol. 106, 2023. [Online]. Available: (https://link.springer.com/article/10.1007/s00202-023-01795-6)
18. E. Shirzad, "Analytical model for double-sided linear permanent magnet inner armature synchronous machine with slot-less stator at on-load in different patterns of magnetization," *Electrical Engineering*, 2023. [Online]. Available: (https://link.springer.com/article/10.1007/s00202-023-01904-5)

AUTHOR'S PROFILE

Ehsan Shirzad, I was born in Bojnord in 1994. I graduated from Shiraz University of Technology (PhD) in 2021, and my research interests are in the modelling and optimisation of electrical machines, especially permanent-magnet machines. I am an instructor at the University of Bojnord, where I have taught all courses. Also, I have authored 24 published articles with an h-index of 9, which can be found below https://www.researchgate.net/profile/Ehsan-Shirzad-2?ev=hdr_xprf.

Disclaimer/Publisher's Note: The statements, opinions and data contained in all publications are solely those of the individual author(s) and contributor(s) and not of the Blue Eyes Intelligence Engineering and Sciences Publication (BEIESP)/ journal and/or the editor(s). The Blue Eyes Intelligence Engineering and Sciences Publication (BEIESP) and/or the editor(s) disclaim responsibility for any injury to people or property resulting from any ideas, methods, instructions, or products referred to in the content.

© Copyright: All rights reserved.